Fermi National Accelerator Laboratory

FN-406
1100.700
(Submitted to Health Physics)

RADIATION MEASUREMENTS IN A LABYRINTH PENETRATION AT A HIGH ENERGY PROTON ACCELERATOR

J. D. Cossairt, J. G. Couch, A. J. Elwyn, and W. S. Freemán

July 1984

Operated by Universities Research Association Inc. under contract with the United States Department of Energy

RADIATION MEASUREMENTS IN A LABYRINTH PENETRATION AT A HIGH ENERGY PROTON ACCELERATOR

J.D.Cossairt, J.G.Couch, A.J.Elwyn, and W.S.Freeman
Fermi National Accelerator Laboratory*
Batavia, Illinois 60510 USA

ABSTRACT

The efficient design of access penetrations at high energy proton accelerators is desirable for both economic and personnel protection reasons. This paper reports on a series of measurements made in a personnel access labyrinth which viewed an aluminum target bombarded by 400 GeV protons from the Fermilab Tevatron. Measurements of absorbed dose rates in the labyrinth using tissue equivalent ion chambers were consistent with theoretical predictions of both the relative attenuation through the penetration and the absolute magnitude near the target. The multisphere technique was used to determine the neutron energy spectrum in one section of the labyrinth. A recombination chamber was used to measure the quality factor of the radiation field in two sections of the labyrinth. Good agreement with the quality factor deduced from the multisphere result was obtained at the same measurement location.

*Operated by Universities Research Association, Inc. under contract with the U.S.Department of Energy.

1. Introduction

Compared with other aspects of the design of shielding of high energy accelerators, the radiation fields in access penetrations have received rather scant attention in the published literature, particularly for multihundred GeV proton accelerators. A summary of the work prior to 1973 is given in the classic text of Patterson and Thomas (Pa73). Two other older references are those of Stevenson and Squier (St73) and Gollon and Awschalom (Go71). More recently, Tesch has found empirical formulae which describe existing measurements of attenuation of dose equivalent by labyrinths quite well (Te82). The present work discusses measurements made in a particular labyrinth at Fermilab.

2. Geometry of the Access Penetration Under Study

Figure 1 shows the geometry of the labyrinth which is made of four straight sections ("legs"). For these legs, coordinates r_i are defined as shown. Leg 1 is buried under an earth shield while legs 2,3 and 4 are made of concrete shielding blocks. Leg 4 (outdoors) has no roof. An extracted beam of 400 GeV protons from the Fermilab Tevatron was centered on an aluminum target of square cross section (0.15 m x 0.15 m) by 0.3 m long (roughly a collision length for high energy protons). The beam of protons and high energy reaction products continued in a 0.9 m diameter vacuum pipe (not shown in Figure 1) 76 meters past the target without further interactions. Emerging from the aluminum vacuum box lid (0.025 m thick) were neutrons and photons produced at large angles relative to the incident proton beam or scattered

from the walls of the vacuum chamber. A secondary emission monitor (SEM), accurate to about $\pm$ 5% was used to measure the proton beam intensity (typically 2×10^{11} during a 15 sec beam spill) delivered to the target once every 39 sec. The Gaussian beam profile had a full width at half maximum of 1.4 cm in both transverse coordinates.

3. Absorbed Dose Rate Measurements and Predictions

Tissue equivalent ion chambers of Fermilab design and calibration, placed near the center of the enclosure at a nominal height of 1.2 m above the floor, were used to measure the absorbed dose rate at a number of locations in the labyrinth. Data from as many as six locations throughout the labyrinth were taken simultaneously by reading out current digitizers (one pulse/0.5 μrad) on scalers. For one set of measurements a bending magnet was used to move the beam across the target, and thus vary the intensity striking it by a factor of about 100 using the spatial profile of the beam. During this scan, the responses of the detectors relative to each other were constant to within about 10 per cent, verifying the linearity over this dynamic range. The measurements of absorbed dose are shown as the solid circles in Figure 2 where the error bars indicate systematic uncertainties traceable to various nonreproducibilities of the beam targetry.

It is, of course, desirable to be able to reliably predict these absorbed dose rates. Gollon and Awschalom (Go71) have reported a number of Monte-Carlo calculations of labyrinth attenuation using the albedo program ZEUS of F.Gervaise and M.-M. d'Hombres (Ge68, dH68). In this program monoenergetic

neutrons (3 or 4 MeV) were scattered at random angles from the walls of "typical" labyrinths using dose albedo parameters of Maerker and Muckenthaler (Ma65). The dashed curve in Figure 2 was obtained by applying these results to the labyrinth at hand and arbitrarily normalizing to the measured absorbed dose rate at r_1 = 1.98 m, the "mouth" of the first leg, where the beam enclosure narrows down to the passageway. Agreement between this calculation and the measurements is quite good; the disagreement is only a factor of three at the end of leg 4. This arises for the most part in leg 3 and may be due to the fact that the very short second leg barely occludes the source.

Tesch (Te82) presents two empirical formulae which describe existing data of the attenuation of dose equivalent in labyrinths. One is appropriate for describing the attenuation in a labyrinth section which is directly exposed to the source. It is an inverse square law dependence which Tesch determined is adequate, if suitably normalized, even if scattering from the walls is taken into account, and is restated here as Eq (1):

$$H(r_1) = 2\, H_o(a) a^2 r_1^{-2} \qquad (1)$$

In this expression, $H(r_1)$ is the dose equivalent rate at coordinate r_1 in the first leg, a is the distance from the source to the mouth of the first section (here a = 1.98 m), and $H_o(a)$ is the calculated dose equivalent rate at distance a from a point source of given strength. The factor of two represents an estimate of the contribution of wall scattering to the total dose equivalent at r_1. For the attenuation of successive legs (i>1), Tesch presents a simple sum of two exponentials,

$$H(r_i) = \frac{[\exp(-r_i/0.45) + 0.022\ A_i^{\ 1.3}\ \exp(-r_i/2.35)]}{[1 + 0.022\ A_i^{\ 1.3}]} \qquad (2)$$

where A_i is the cross sectional area of the enclosure in m^2 and r_i is in meters.

In the present work, the factor of 2 in Eq.(1) was replaced by correction factors for scattering from the floor, walls, and ceiling of leg 1 according to the recipe of Jenkins (Je80). This modification increased the calculated dose rate by about 10 percent at the end of the first leg (at r_1 = 7.48 m). Eq. (2) was used for legs 2 through 4 without modification. It is implicitly assumed that attenuation of absorbed dose mimics that of the dose equivalent. The solid curve in Figure 2 shows the attenuation calculated according to these formulae (again normalized to the measurements at r_1 = 1.98 m). It was assumed that the first leg behaves the same as a leg directly viewing the source (the aluminum target), an approximation since the target was beneath the floor of the enclosure. Agreement of these formulae both with predictions taken from (Go71) and with the measurements is quite good, considering their simplicity. To test for deviations from an inverse square law dependence in the first leg, $r_1^2 D$ (where D is the absorbed dose rate) is plotted as a function of r_1 in Figure 3. The data is adequately described by a horizontal line indicative of an inverse square dependence.

The Monte-Carlo hadronic cascade program CASIM (Va75) was used to calculate the absorbed dose rates above the source by determining the specific energy deposition in a water phantom. This code has been successfully tested experimentally for both thick and thin shields (Aw76, Co82). A prediction of the absorbed dose rate directly above the vacuum chamber lid, centered over the target, is indicated on Figure 2. Also, a calculation of the areal integral of the absorbed dose rate over the lid is compared with the data in Figure 3. For both calculations the indicated errors are representative of the statistics of the Monte-Carlo procedure. The results are in good agreement with the present measurements.

4. Neutron Energy Spectrum Measurement Using the Mulisphere Technique

a) Experimental Method

The multisphere technique (Br60, Aw84) was used to obtain information on the neutron spectrum at r_2 = 1.23 m. Neutrons were moderated by polyethylene spheres of several radii (r = 2.54, 3.81, 6.35, 10.2, 12.7, and 15.2 cm). ^{6}LiI(Eu) scintillators, sensitive to thermal neutrons through the ^{6}Li(n,α)t (Q-value = 4.78 MeV) reaction, were placed at the center of the moderating spheres and inserted two at a time into the labyrinth. A measurement was also made with a bare (unmoderated) scintillator. The ^{6}LiI(Eu) crystal (8 mm diam. by 8 mm long) was embedded in a small amount of plastic scintillator (12.7 mm by 12.7 mm), and the light output from both was viewed by a single photomultiplier tube. This phoswich detector has been described previously by Awschalom (Aw73). Fast pulses (2-3 nsec) from the plastic scintillator were

separated from the slow (1-2 μsec) pulses of the ^{6}LiI(Eu) by passive filtering at the phototube output. Standard pulse-processing electronics were used to accumulate a spectrum of all slow pulses in anti-coincidence with fast signals. This method rejects events due to the passage of charged particles (e.g., muons) through the ^{6}LiI(Eu), reducing the background. A portion of a typical pulse-height spectrum of accepted events near the 4.78 MeV thermal capture peak is shown in the insert of Figure 4.

The detectors were gated on only during the 15 second beam spills, and a tissue equivalent ionization chamber located at r_1 = 7.4 m provided the relative nomalization. Spill-to-spill variations in the normalized counts were less that 2%, and data was accumulated for five beam spills per sphere. The filled circles in Figure 4 are the results based on measurements for each sphere. The open circles and crosses are calculated results for two different assumed neutron spectra discussed below.

b) Spectrum Unfolding

Multisphere spectrum-unfolding techniques have been discussed by many authors (Ob81, Ch83, Ob83, Gr73, Aw84) and we only summarize this problem here. The counting rate C_r of a thermal neutron detector at the center of a spherical moderator of radius r is given by

$$C_r = \int_0^\infty \frac{dN}{dE} R_r (E) dE \qquad (3)$$

Given C_r and $R_r(E)$ the problem is to find dN/dE. In practice, one uses a discrete approximation to Eq. (3) by converting the integral to a sum,

$$C_r = \sum_i \frac{dN}{dE_i} R_r (E_i)\Delta E_i \quad , \tag{4}$$

where (dN/dE_i) is the differential neutron energy flux for the ith energy group. The response functions $R_r(E_i)$ are obtained by separate calculations. We have used those of Sanna (Sa73) appropriate for our 8 mm x 8 mm LiI(Eu) crystals and modified for polyethylene spheres of density 0.92 g/cm^3. The C_r values are proportional to the measured quantities shown in Figure 4.

As is well known, the spectrum unfolding problem has inherent difficulties, due to its underdetermined and sometimes ill-conditioned nature (Gr73, Ch83). The former manifests itself as more than one solution spectrum that describes the data equally well, while the latter implies that small uncertainties in the data or response functions may translate into large uncertainties in the unfolded spectrum.

We have chosen to use the Monte Carlo code SWIFT (OB81) to derive possible neutron spectra that reproduce the data in Figure 4, rather than the iterative techniques that are often employed (Gr73). The Monte Carlo method allows a broad sampling of possible neutron spectra with no a priori assumptions about the character of the spectrum (other than its positivity).

Figure 5 displays the unfolded spectrum that was obtained from a bin-by-bin averaging of the four spectra that best described the data. A total of 9.3×10^6 sample spectra were generated in order to obtain this result. The error bars represent the standard deviation in the spectrum values obtained from the averaging procedure. Note that the energy scale (abscissa) is logarithmic and the ordinate is dN/d(log E). Such a plot has the advantage that it preserves the relative area representation of the spectrum (IC69, Ro83). Thus, visual integration of the area under the curve for each energy bin is possible, and this area is proportional to the neutron fluence within that bin.

The characteristic feature of the unfolded spectrum is that 72% of the total neutron fluence is within the "thermal" or lowest energy bin. While the fraction within the thermal bin seems to be well determined, the distribution of the remaining fluence is highly uncertain.

It is not surprising that the spectrum in the second leg of the labyrinth is dominated by thermal neutrons, because of the multiple scattering that must take place in order to reach the detector. However, it is also clear that non-thermal (>0.4 eV) neutrons are present. The open circles in Fig.4 represent calculated ball counts if 100% of the fluence was assumed to be in the thermal bin. The deviations between the calculated and measured points are much greater than the statistical errors associated with the data (2%). In contrast, the calculated ball counts for the unfolded average spectrum (crosses) agree to better than 6% with the data. Finally, we note that the calculated quality factor of the unfolded spectrum is 3.1 ± 0.7.

5. Quality Factor Measurements Using a Recombination Chamber

The use of columnar recombination to measure the quality factor (QF) of mixed fields of radiation has been described by Sullivan and Baarli (Su63) and summarized by Patterson and Thomas (Pa73). Measurements were done at two locations in this labyrinth; near the end of the first leg, (r_1 = 7.4 m) and in the middle of the second leg (r_2 = 0.85 m). To determine the quality factor in this manner, the response of a commercial high pressure ion chamber specifically designed for this purpose (REM-2 Chamber ZZUJ "Polon" Radiation Dosimetry Instrument Division, Bydgoszcz, Poland) was measured over its operating voltage range (≤1200 volts). According to Sullivan and Baarli (Su63), the following equation will describe the response function of such a chamber

$$I = kV^N, \tag{5}$$

where I is the measured current or charge collected at the anode at chamber potential V (using some appropriate means of normalization) and k is a constant of proportionality dependent upon the chamber used. The exponent N depends upon the average LET of the radiation field and is thus correlated with the average quality factor.

In order to understand the response of the particular chamber used, the value of I as a function of V was measured in a variety of radiation fields having QF values ranging from unity (^{60}Co gamma rays) to 6.9 (^{238}Pu-Be source, including the gamma ray component (Ho80)). For each set of data, the value of N was determined from Eq. (5) by the method of least squares. The relationship between N and QF is shown in Figure 6 along with both power law and linear fits to these points. Both fits miss the datum at QF=1. At these small values of QF, the change in the charge collected at the anode for a given change in the chamber potential becomes quite difficult to measure accurately because N in Eq. (5) is so small. (Co84) describes measurements using this chamber in more detail.

Figure 7 shows response functions measured in the first and second legs of the labyrinth (normalized to the absorbed dose measured by one of the ion chambers placed very near to the recombination chamber). The value of QF = 5.5 $\pm$ 0.6 found at r_1 = 7.4 m agrees with expectations, since it is exposed to the relatively energetic neutron spectrum emerging from the source, while that obtained in the second leg (QF = 3.4 $\pm$ 0.1) is consistent with the results obtained from the spectrum measurement described in Section 4.

6. Conclusions

It is concluded that reasonable estimates of absorbed dose rate attenuation in personnel labyrinths for radiation protection purposes may be made using two different methods one of which involves simple empirical formulae. The use of a Monte Carlo cascade calculation to correctly predict

the absolute magnitude of these absorbed dose rates has been verified. The neutron energy spectrum obtained with the multisphere technique, even with the uncertainties inherent in the unfolding procedure, is still useful in the determination of the average quality factor. The value is in good agreement with that obtained using the recombination chamber.

We would like to thank V.Frohne, S.Pordes, and L.Stutte for their help in obtaining these data.

REFERENCES

Aw73 Awschalom M., and Coulson L., 1973, "A New Technique in Environmental Neutron Spectroscopy", Proc. Third International Congress of IRPA, Washington, D.C., 1464-1469.

Aw76 Awschalom M., Baker S., Moore C., Van Ginneken A., Goebel K., and Ranft J., 1976, "Measurements and Calculations of Cascades Produced by 300 GeV Protons Incident on a Target Inside a Magnet", Nucl.Instr. and Meth. 138, 521-521.

Aw84 Awschalom M., and Sanna R., 1984, "Applications of Bonner Sphere Detectors in Neutron Fields", Private Communication, to appear in Radiation Protection and Dosimetry.

Br60 Bramblett R.L., Ewing R.I., and Bonner T.W., 1960, "A New Type of Neutron Spectrometer", Nucl.Instr. and Meth.9, 1-12.

Ch83 Chambless D.A., and Broadway J.A., 1983, "Comments On Neutron Spectral Unfolding Using the Monte Carlo Method", Nucl.Instr. and Meth.214 543-545.

Co82 Cossairt J.D., Mokhov N.V., and Murphy C.T., "Absorbed Dose Measurements External to Thick Shielding At a High Energy Proton Accelerator: Comparison with Monte-Carlo Calculations", Nucl.Instr.and Meth.197, 465-472.

Co84 Cossairt J.D., Grobe D.W., and Gerardi M.A., 1984, "Measurements of Radiation Quality Factors Using a Recombination Chamber", Fermilab Report TM-1248, Fermilab, Batavia Il 60510.

dH68 d'Hombres M.M., Devillers C., Gervaise F., de Sereville B., Tardy-Joubert PH., 1968, "Propagation des Neutrons dans les Tunnels d'Acces a un Accelerateur de Haute Energie a Protons", G.6802-AIR.41-NC.

Ge68 Gervaise F., and d'Hombres M.-M., 1968, "Variate du Programme ZEUS Appliquee a des Problemes de Tunnels", C.E.N. Fontenay-aus- Roses, Note CEA-N-933.

Go71 Gollon P.J., and Awschalom M., 1971, "Design of Penetrations in Hadron Shields", IEEE Trans.Nucl.Sci.NS-18, 741.

Gr73 Grunauer F., and Schmatz W., 1973, "Data Analysis for Low Resolution Neutron Spectrometry", and references therein, IAEA, Neutron Monitoring for Radiation Protection Purposes, Vol.I, SM-167/31, 59-71.

Ho80 Höfert M., and Raffnsøe C., 1980, "Measurement of Absolute Absorbed Dose and Dose-Equivalent Response for Instruments Used Around High Energy Proton Accelerators", Nucl.Instr.and Meth., 176, 443.

IC69 ICRU Report 13, 1969, "Neutron Fluence Neutron Spectra and Kerma", International Commission on Radiation Units and Measurements, Washington, D.C.

Je80 Jenkins T.M., 1980, "Simple Recipes for Ground Scattering in Neutron Detector Calibrations", Health Phys.39, 41-47.

Ma65 Maerker R.E., and Muckenthaler F.J., 1965, "Calculation and Measurement of the Fast- Neutron Differential Dose Albedo for Concrete", Nucl.Sci.Eng.22, 465.

OB81 O'Brien K., and Sanna R., 1981, "Neutron Spectrum Unfolding Using the Monte Carlo Method", Nucl.Instr.and Meth.185, 277-286.

OB83 O'Brien K., and Sanna R., 1983, "Reply to Chambless and Broadway", Nucl.Instr.and Meth.214, 547-549.

Pa73 Patterson H. Wade., and Thomas R.H., 1973, Accelerator Health Physics (New York: Academic Press).

Ro83 Rohrig N., 1983, "Plotting Neutron Fluence Spectra", Health Phys.45, 817-818.

Sa73 Sanna R.S., 1973, "Thirty One Group Response Matrices for the Multisphere Neutron Spectrometer Over the Energy Range Thermal to 400 Mev", U.S. AEC, HASL-267.

St73 Stevenson G. R., and Squier D. M., 1973, "An Experimental Study of Attenuation of of Radiation in Tunnels Penetrating the Shield of an Extracted Beam of the 7 GeV Proton Synchrotron NIMROD", Health Phys.24, 87-93.

Su63 Sullivan A. H., and Baarli J., 1963, "An Ionization Chamber for the Estimation of the Biological Effectiveness of Radiation", CERN Report No.63-17 (European Organization for Nuclear Research, Geneva).

Te82 Tesch K., 1982, "The Attenuation of the Neutron Dose Equivalent in a Labyrinth Through an Accelerator Shield", Particle Accelerators 12, 169-175.

Va75 Van Ginneken A., and Awschalom M., 1975, High Energy Particle Interactions in Large Targets, Vol.1 (Fermilab, Batavia, Il.).

FIGURE CAPTIONS

Figure 1 Plan and elevation views of the access labyrinth studied. Coordinates used in the text are defined in this figure.

Figure 2 Absorbed dose rate measurements and predictions plotted as a function of labyrinth coordinates. A Monte-Carlo prediction for the absorbed dose rate directly above the target is also shown.

Figure 3 Absorbed dose rate in leg 1, D, multiplied by r_1^2 plotted as a function of r_1. A Monte-Carlo calculation of the areal integral of absorbed dose rate over the vacuum box lid is also shown.

Figure 4 Normalized counts from the phoswich detector for each spherical moderator. The solid points are the labyrinth data. The open circles represent calculated results assuming a purely thermal spectrum while the crosses are the results for the averaged spectrum unfolded using the code SWIFT. The solid and dashed curves are drawn to guide the

eye. The insert shows a typical gated spectrum of the pulse heights in the ^{6}LiI(Eu).

Figure 5 The unfolded neutron spectrum in the second labyrinth leg, plotted as fluence per unit of logarithmic interval. Error bars represent the uncertainty in the spectrum obtained from the averaging procedure described in the text.

Figure 6 Recombination chamber measurements of the relationship between N and QF using radioactive sources. Two different equations used to fit these data are plotted.

Figure 7 Recombination chamber response functions measured at two different locations in the labyrinth.

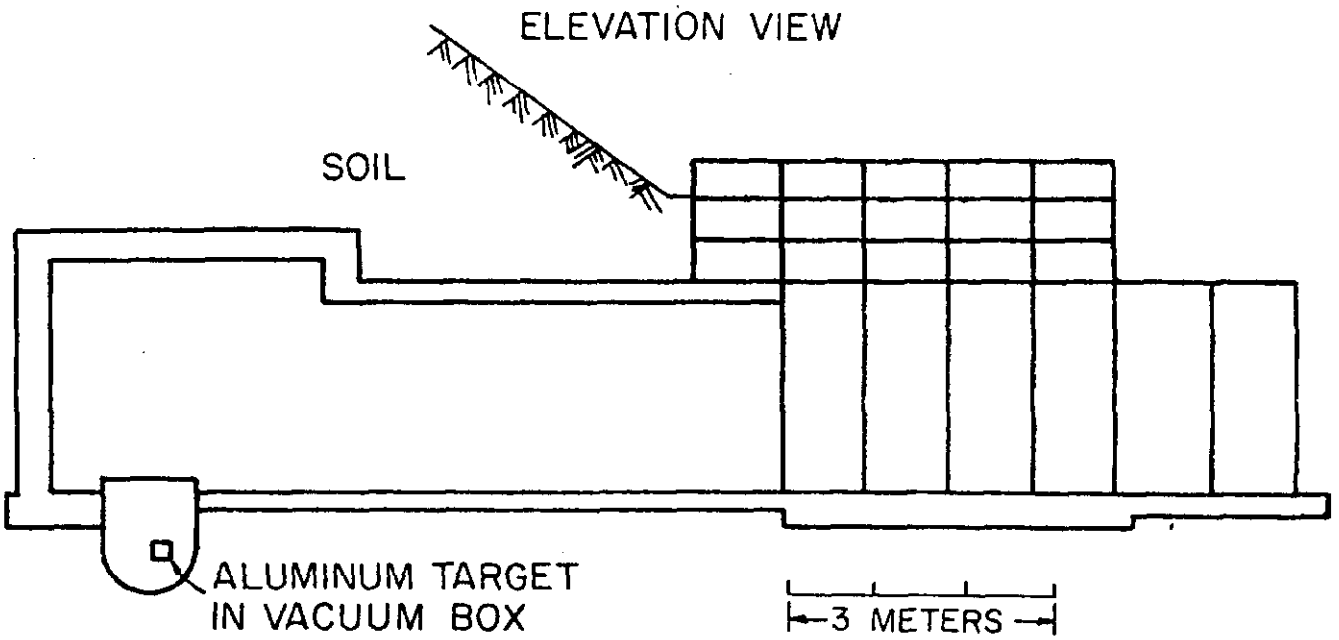
ELEVATION VIEW
SOIL
ALUMINUM TARGET
IN VACUUM BOX
3 METERS

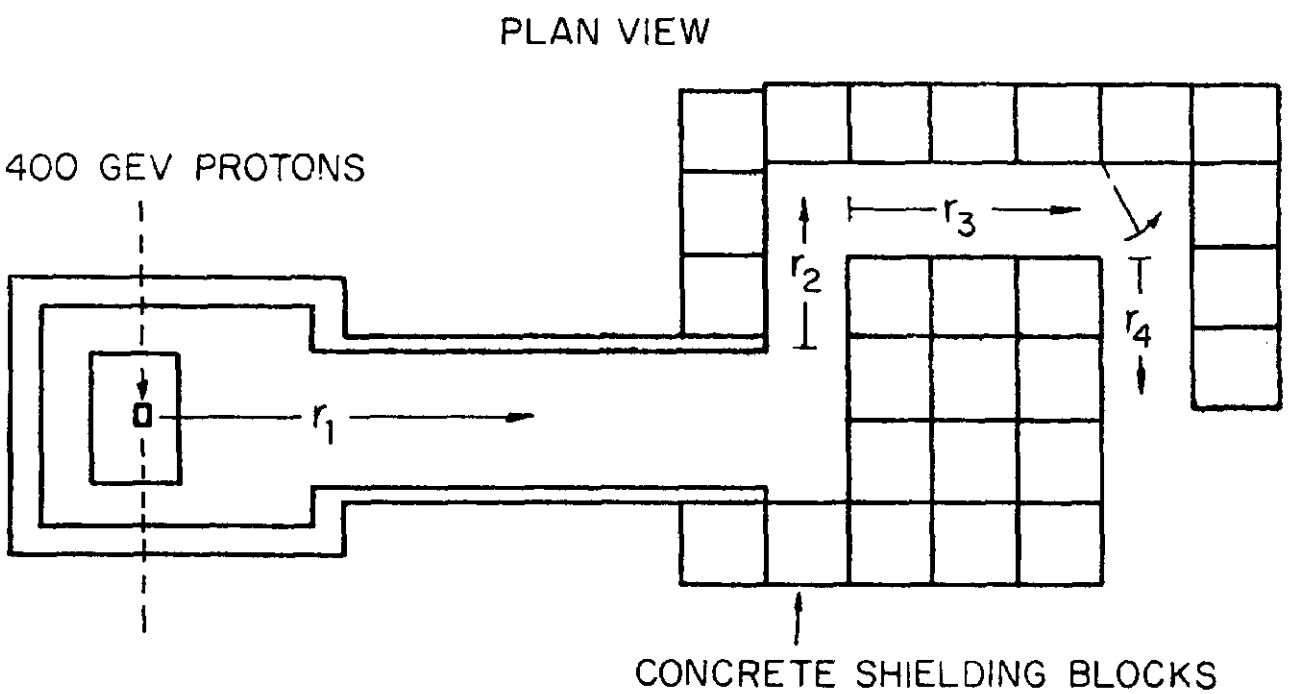
PLAN VIEW
400 GEV PROTONS
r_1
r_2
r_3
r_4
CONCRETE SHIELDING BLOCKS

Figure 1

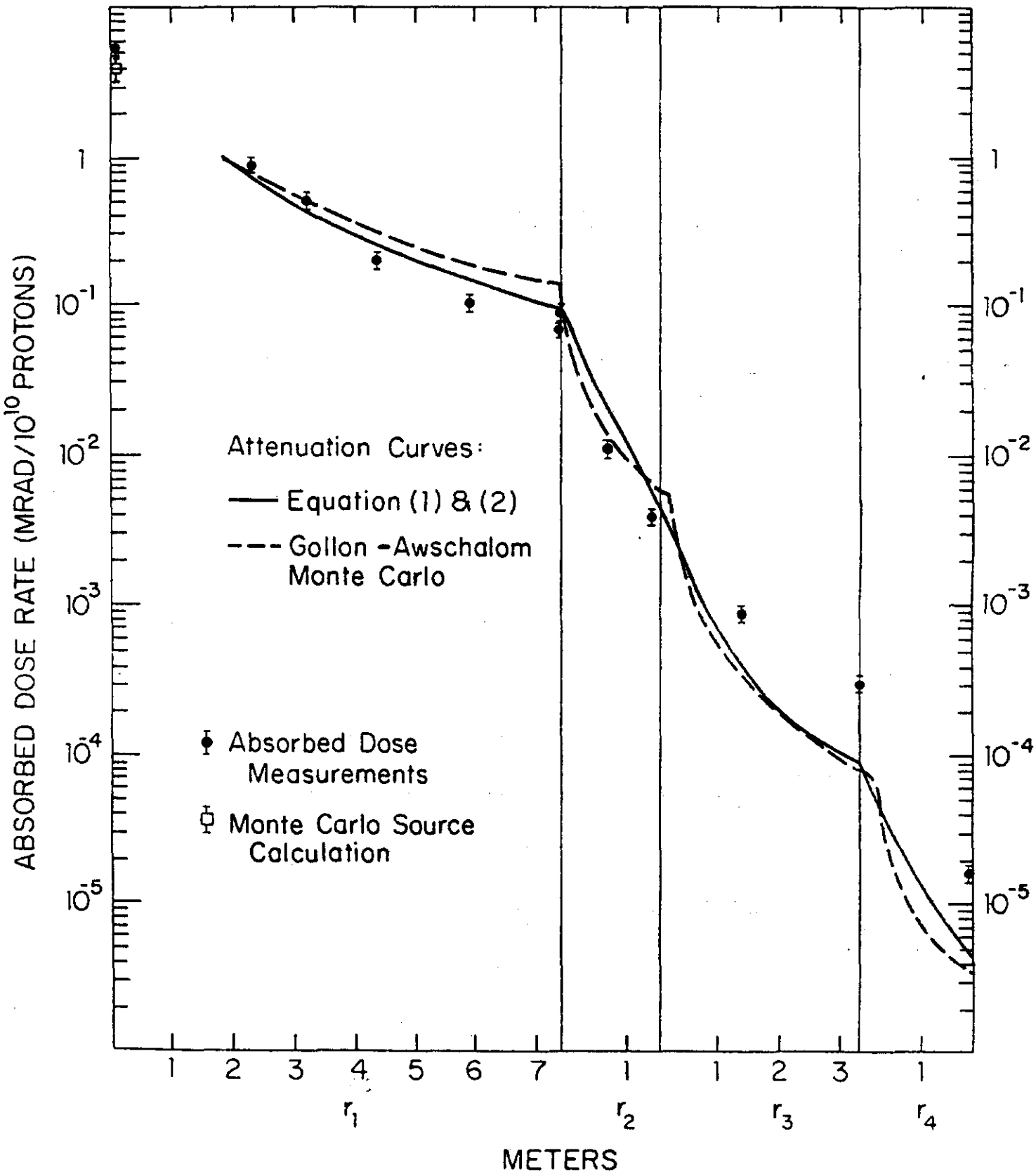
ABSORBED DOSE RATE (MRAD/10^10 PROTONS)
1
10^-1
10^-2
10^-3
10^-4
10^-5
Attenuation Curves:
Equation (1) & (2)
Gollon -Awschalom Monte Carlo
Absorbed Dose Measurements
Monte Carlo Source Calculation
1 2 3 4 5 6 7
r1
1
r2
1 2 3
r3
1
r4
METERS

Figure 2

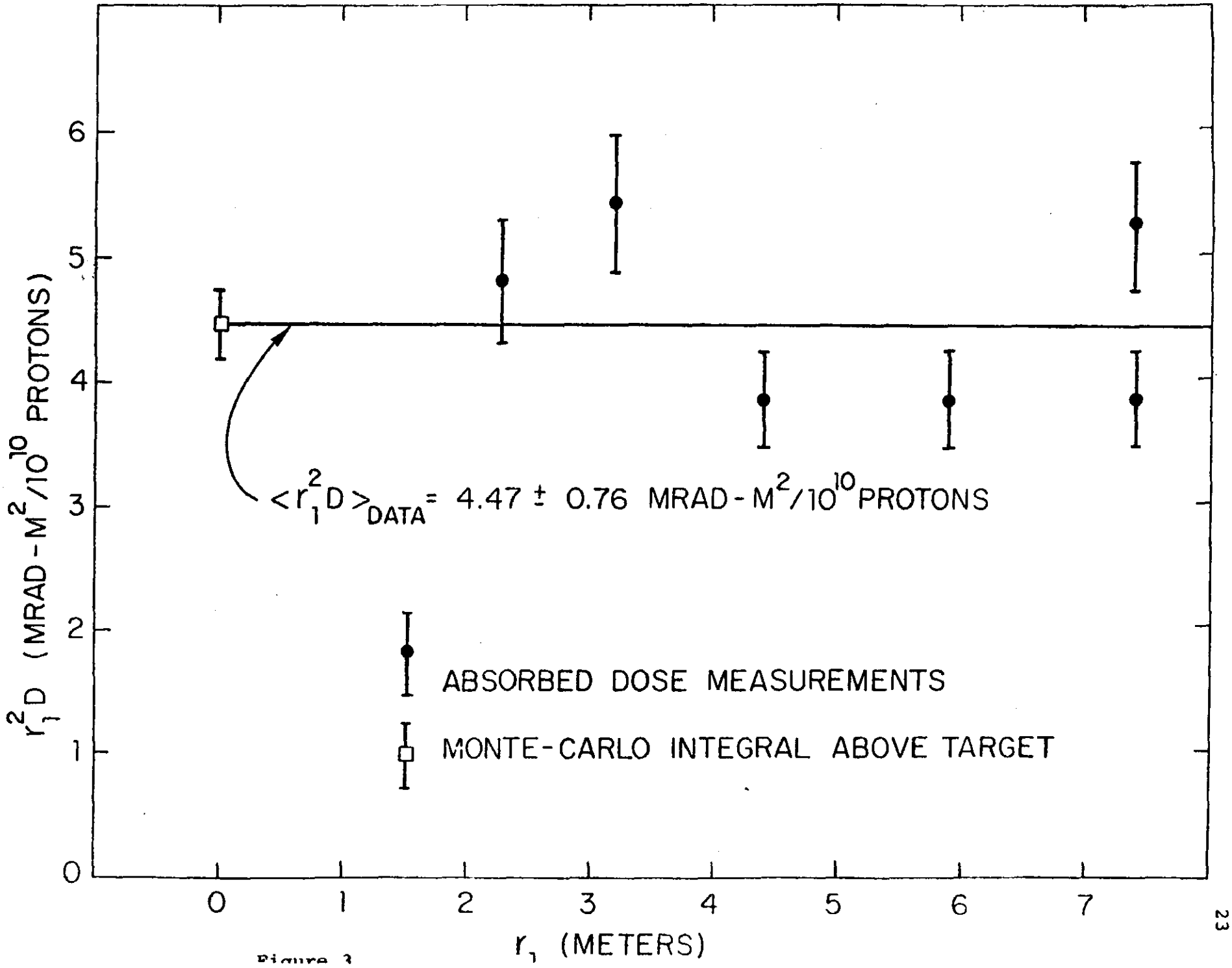
$r_1^2 D$ (MRAD-M^2/10^{10} PROTONS)
r_1 (METERS)
$\langle r_1^2 D \rangle_{DATA}$ = 4.47 ± 0.76 MRAD-M^2/10^{10} PROTONS
ABSORBED DOSE MEASUREMENTS
MONTE-CARLO INTEGRAL ABOVE TARGET
0
1
2
3
4
5
6
7

Figure 3

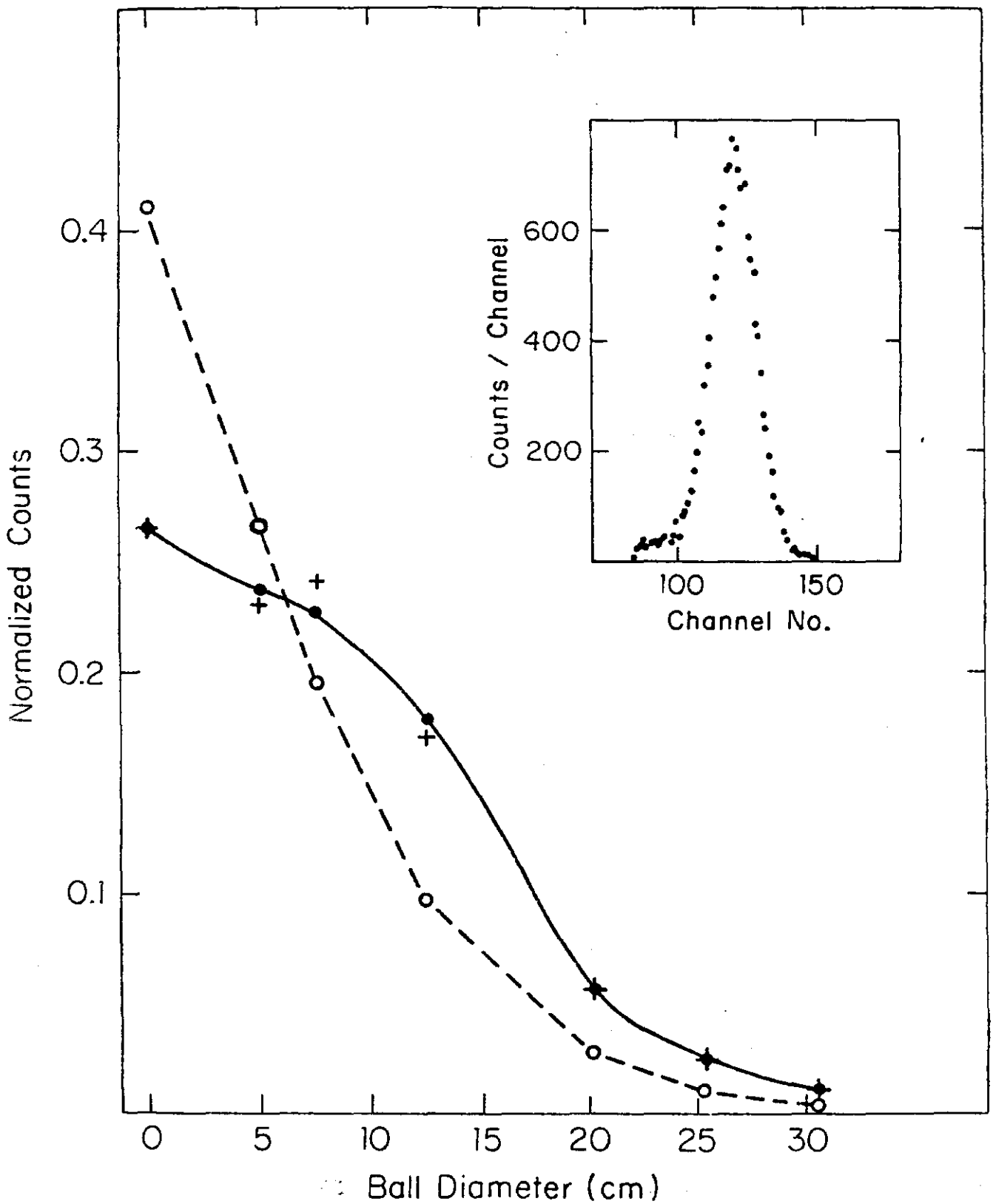
0.4
0.3
0.2
0.1
Normalized Counts
0
5
10
15
20
25
30
Ball Diameter (cm)
600
400
200
Counts / Channel
100
150
Channel No.

Figure 4

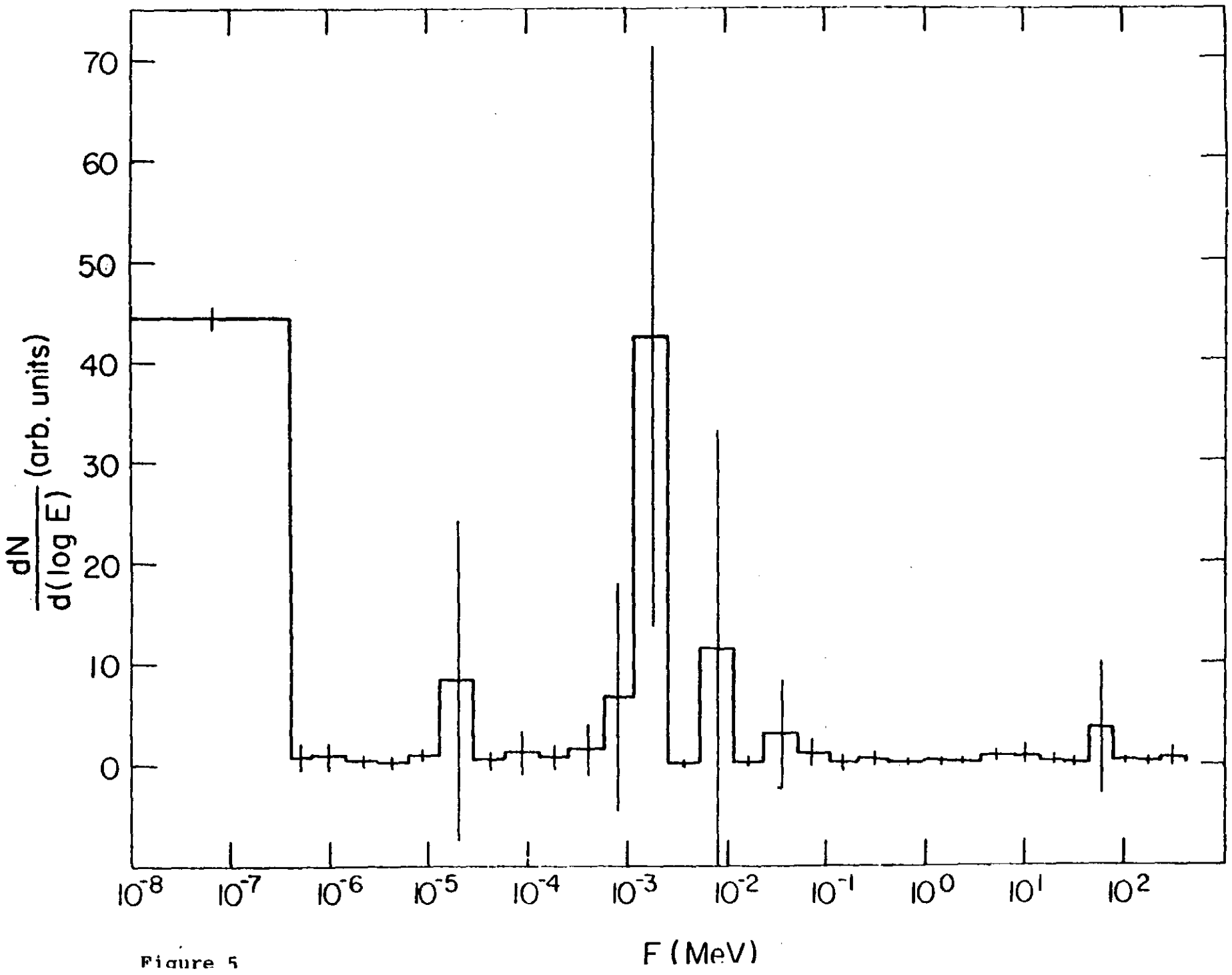
70
60
50
40
30
20
10
0
dN / d(log E) (arb. units)
10^-8
10^-7
10^-6
10^-5
10^-4
10^-3
10^-2
10^-1
10^0
10^1
10^2
F (MeV)

Figure 5

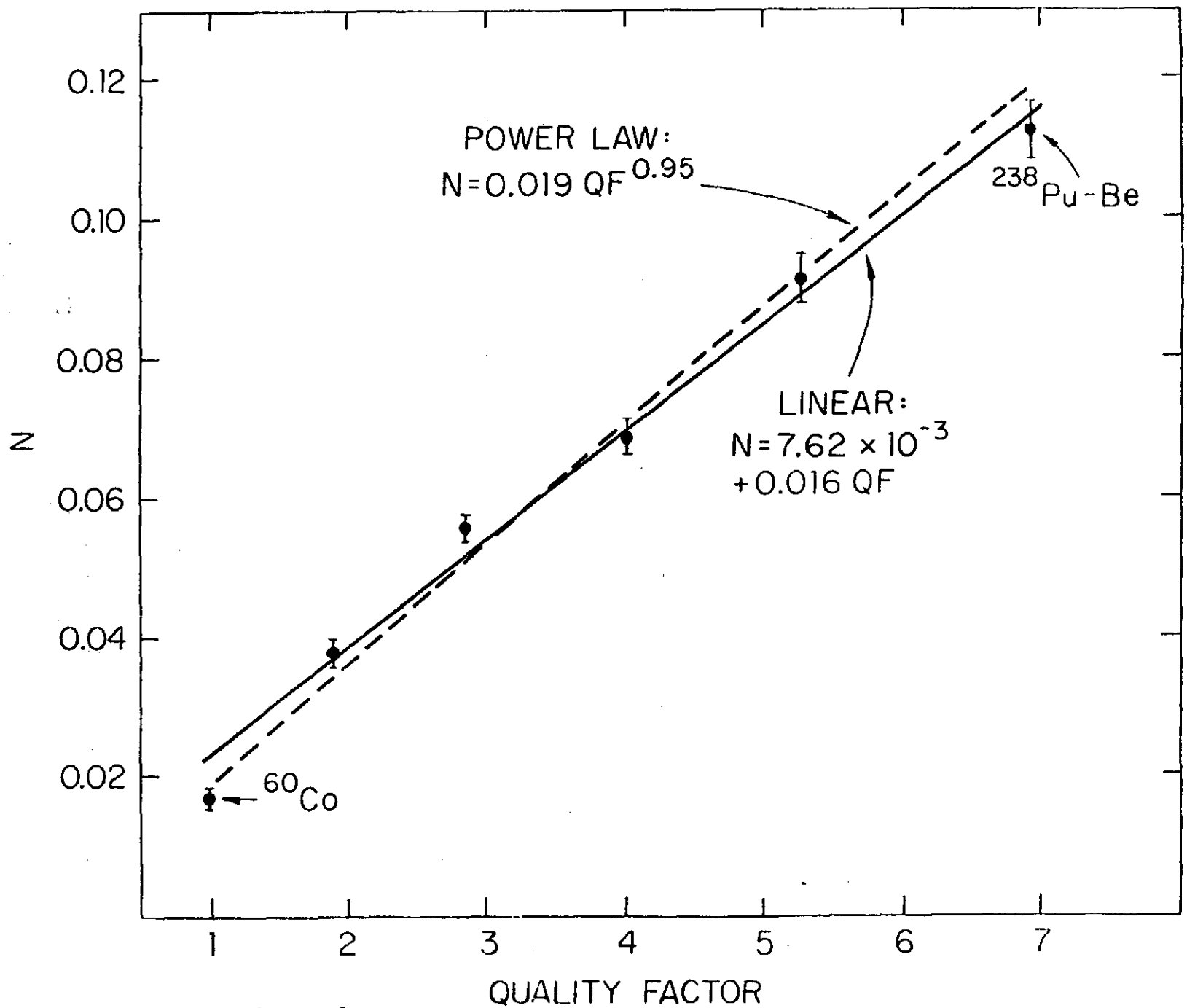
0.12
0.10
0.08
0.06
0.04
0.02
N
POWER LAW:
N=0.019 QF^0.95
LINEAR:
N=7.62 × 10^-3
+0.016 QF
238Pu-Be
60Co
1
2
3
4
5
6
7
QUALITY FACTOR

Figure 6

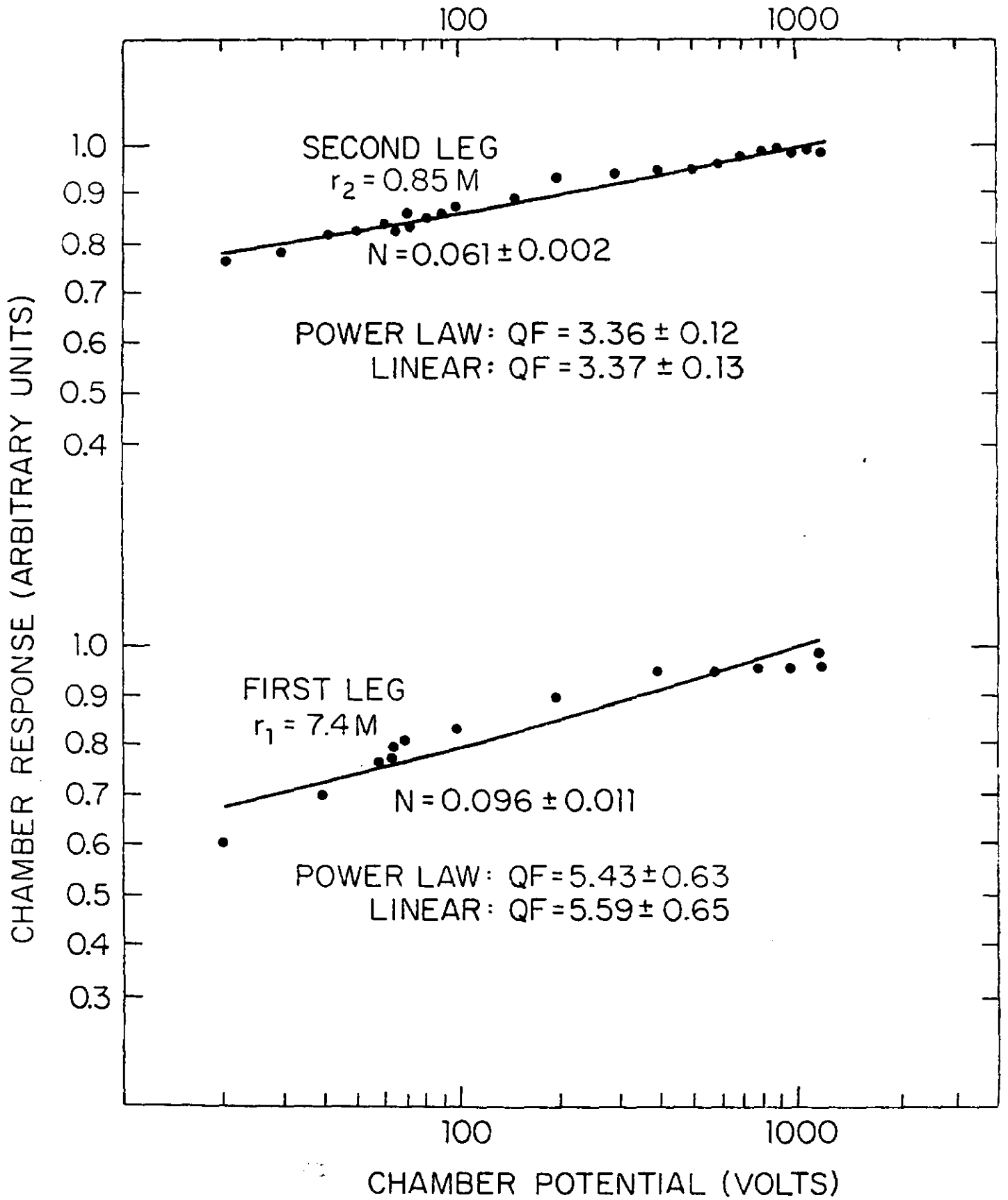
100
1000
SECOND LEG
r_2 = 0.85 M
N = 0.061 ± 0.002
POWER LAW: QF = 3.36 ± 0.12
LINEAR: QF = 3.37 ± 0.13
FIRST LEG
r_1 = 7.4 M
N = 0.096 ± 0.011
POWER LAW: QF = 5.43 ± 0.63
LINEAR: QF = 5.59 ± 0.65
1.0
0.9
0.8
0.7
0.6
0.5
0.4
0.3
CHAMBER RESPONSE (ARBITRARY UNITS)
CHAMBER POTENTIAL (VOLTS)

Figure 7